Spin-Reorientation-Induced Band Gap in Fe_3Sn_2: Optical Signatures of Weyl Nodes

A. Biswas,[1] O. Iakutkina,[1] Q. Wang,[2] H. C. Lei,[2,*] M. Dressel,[1] and E. Uykur[1,†]
[1]1. Physikalisches Institut, Universität Stuttgart, 70569 Stuttgart, Germany
[2]Department of Physics and Beijing Key Laboratory of Opto-electronic Functional Materials & Micro-nano Devices, Renmin University of China, Beijing 100872, China

(Received 3 April 2020; accepted 21 July 2020; published 12 August 2020)

Temperature- and frequency-dependent infrared spectroscopy identifies two contributions to the electronic properties of the magnetic kagome metal Fe_3Sn_2: two-dimensional Dirac fermions and strongly correlated flat bands. The interband transitions within the linearly dispersing Dirac bands appear as a two-step feature along with a very narrow Drude component due to intraband contribution. Low-lying absorption features indicate flat bands with multiple van Hove singularities. Localized charge carriers are seen as a Drude peak shifted to finite frequencies. The spectral weight is redistributed when the spins are reoriented at low temperatures; a sharp mode appears suggesting the opening of a gap due to the spin reorientation as the sign of additional Weyl nodes in the system.

DOI: 10.1103/PhysRevLett.125.076403

Magnetic kagome metals are emerging as a new class of materials with special crystal structures, which are supposed to bring together electronic correlations, magnetism, and topological orders [1]. Merging the strong electronic correlations with the topologically nontrivial states makes new types of exotic phenomena possible ranging from fractional quantum Hall effect to axion insulators.

Unfortunately, the realization of the materials in this regard is scarce [2–5]. The FeSn-binary compounds are possible candidates; Fe_3Sn_2 is one of them, where the linearly dispersing Dirac bands lying below the Fermi energy are confirmed as well as flat bands around E_F. The crystal structure of Fe_3Sn_2 protects the inversion and threefold rotational symmetry, while the time reversal symmetry is broken due to the magnetic nature of the system. The unique structural properties of this system give rise the flat-band ferromagnetism [6], anomalous Hall effect [7,8], and topological Dirac states [9]. Due to the strong influence of magnetism, a large tunability of the spin-orbit coupling [10] and of the massive Dirac fermions [9,11] was proposed as well as the emergence of further Weyl nodes at the Fermi energy [12].

Fe_3Sn_2 consist of bilayer kagome network separated via stanene layers. The bilayer structure gives rise to the interlayer hybridization due to the multiple d orbitals of Fe atoms leading to deviations from the ideal single-orbital two-dimensional kagome lattice scenario [13–15]. For instance, the flat bands do not extend over the entire Brillouin zone and show a small dispersion [6]; moreover, correlations among the Dirac bands open a gap at the crossing points that give rise to the correlated massive Dirac fermions [9]. Despite these deviations from the ideal scenario, this system provides a beautiful playground for investigating the interplay between magnetism, strong electronic correlations, and topological orders.

For Fe_3Sn_2 it is known that even in the absence of an external magnetic field the spins reorient at reduced temperatures, despite the fact that the system orders ferromagnetically at a much higher temperature, $T \approx 640$ K [16]. The implications of this reorientation on the electronic structure remain an open question. Considering the large sensitivity of magnetism on temperature, here we employ temperature-dependent broadband infrared spectroscopy for studying this model compound. We look for optical fingerprints of Dirac fermions, localized electrons of the flat bands, and spin reorientation, as they directly probe the interplay between these unique states along with the energy scales. In the absence of an external magnetic field, we investigate the effects of the inherent magnetization on the observed properties. Moreover, the high spectral resolution of our technique, even in the low energy range, gives us the opportunity to test theoretical proposals regarding the additional Weyl nodes in the vicinity of E_F.

Single crystals of Fe_3Sn_2 were synthesized as described elsewhere [7]. Here we performed temperature-dependent optical reflectivity measurements on single crystals of Fe_3Sn_2 in a broad energy range. For further details, see the Supplemental Material [17].

Figure 1 displays the temperature-dependent reflectivity along with the optical conductivity in the entire measured range. Consistent with the highly metallic nature of the sample, the low-energy reflectivity reaches almost unity and the optical conductivity approaches the dc conductivity values on the order of 10^5 $(\Omega\,\mathrm{cm})^{-1}$ at low T. While the optical properties are basically temperature independent above approximately 1 eV, a series of interesting features are identified below this energy. (i) A strong suppression of

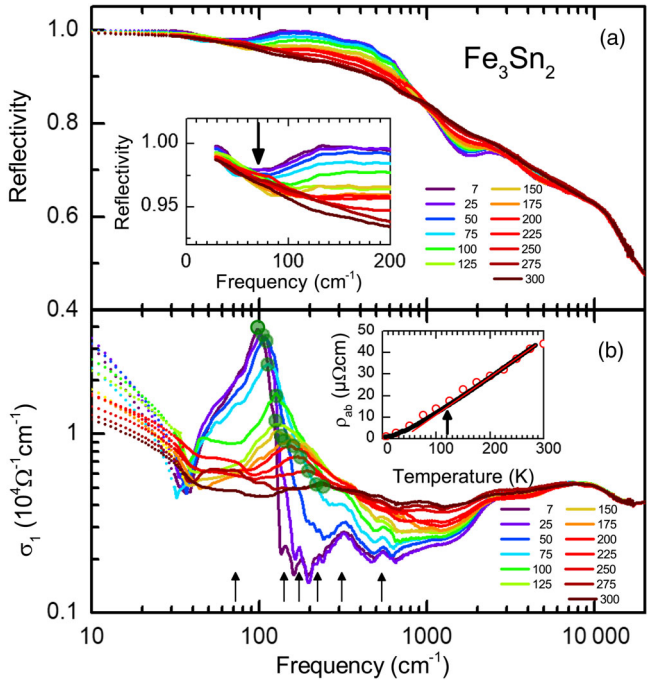

FIG. 1. (a) Temperature-dependent reflectivity of Fe_3Sn_2 in a broad frequency range. The inset magnifies the low-energy reflectivity where the dip causes the peak structure in $\sigma_1(\omega)$. (b) Corresponding optical conductivity at different temperatures. The green circles indicate the peak position. The arrows mark the points of the van Hove singularities. The inset displays the measured dc resistivity of the sample. RRR = 39 indicates the good quality of our sample. The red circles are the dc resistivity values determined via the optical parameters matches very well with the measured resistivity.

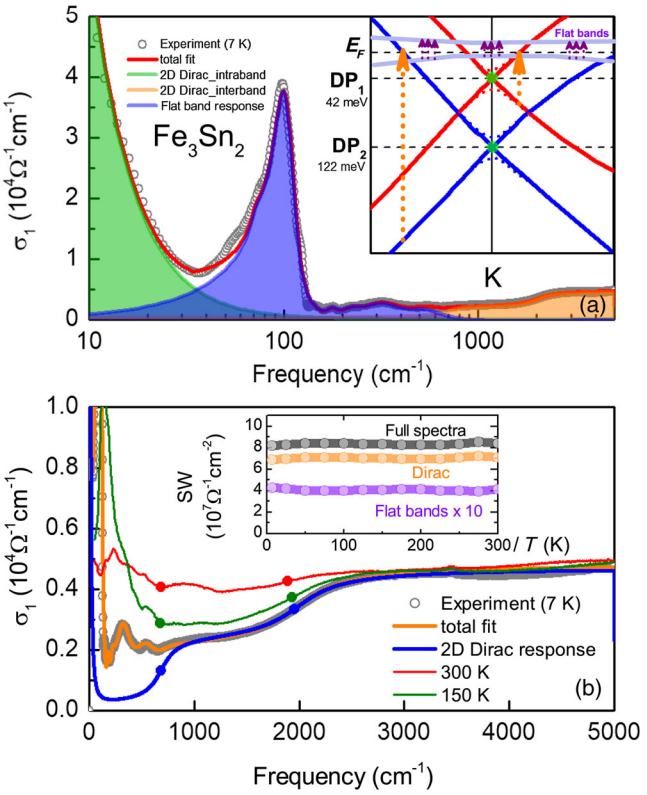

FIG. 2. (a) Decomposition of the 7 K optical conductivity. The red curve represents the fit of the overall spectrum with a Drude (green), flat band responses (blue), and two-dimensional Dirac responses (orange). The inset sketches the band structure along with the transitions. (b) Interband and intraband responses of the two-dimensional Dirac fermions (blue curve) after the flat band contributions have been subtracted from the overall fit. The two step feature and the Dirac points are highlighted. Signs of these points are visible at higher T and do not change significantly with temperature; the $T = 150$ and 300 K spectra are given for comparison. The inset shows the temperature-dependent SW analysis. The details of the fit procedure and the determination of the individual components and their SW can be found in [17].

the reflectivity and, concomitantly, the optical conductivity starting from the midinfrared range. (ii) A peaklike structure (marked with green circles) that shifts to lower energies with decreasing T. (iii) A very narrow Drude component that gets even sharper upon cooling. The scattering of this Drude component is very small and barely visible in our measurement window; however, the dc resistivity data [the inset of the Fig. 1(b)] corroborate its existence [17,21].

We decomposed the optical conductivity into two main parts shown in Fig. 2(a). While the high-energy absorption and the low-energy Drude component can be interpreted within the Dirac fermions framework, the strong absorption features in between have to be treated separately. We attribute these features to the charge carriers within the flat bands, as explained later. This decomposition is supported by the analysis of the spectral weight (SW) [inset of Fig. 2(b)]. The transfer of SW takes place within the different contributions; the overall SW but also the Dirac and the flat-band spectral weights are conserved [17].

But first let us discuss the Dirac physics and its optical signatures in Fe_3Sn_2. The results of angle resolved photoemmision spectroscopy (ARPES) [9,12], scanning tunneling microscopy (STM) [6], and magnetotransport measurements [4,7–9,16] discuss the linearly dispersing bands of massless Dirac fermions and flat bands of massive localized electrons. ARPES data indicate that the Dirac bands lie well below E_F (within ~0.15 eV); whereas the magnetotransport measurements also verify the existence of a topologically nontrivial state. Moreover, the underlying bilayer structure of the kagome lattice gives rise to correlations among the Dirac fermions, causing a correlation gap to open at the Dirac points.

The optical signatures of these Dirac points are clearly visible in our spectra. The midinfrared absorption and the accompanying low-energy Drude component can be well reproduced by taking into account the intraband and interband responses of two-dimensional Dirac fermions as shown in graphene, for instance [22,23]. For a two-dimensional Dirac system with the Dirac point at the Fermi

energy and in the absence of other contributions, the optical conductivity is expected to exhibit a frequency-independent behavior. On the other hand, the shift of the Dirac point with respect to E_F results in absorption feature, where the SW is transferred to the intraband response of the Dirac bands. This situation forbids low energy transitions (up to $2E$, where E defines the energy shift between E_F and the Dirac point) and the optical conductivity starts to increase above a certain energy that is defined as the Pauli edge. In the two-dimensional case, one expects a steplike increase starting from $2E$ and leveling off to the ω-independent behavior [24].

In Fig. 2(b), the 7 K spectrum is plotted with the overall fit to our data, and after subtracting the low-lying absorption features. This remaining part represents the inter- and intraband contributions of the Dirac fermions; the resulting blue curve reproduces the high-energy interband transitions very well. In our case, these high-energy interband transitions involve not one steplike feature but actually two. Hence, a somewhat more complicated picture is present in this system and the response of the Dirac fermions cannot be explained within a single Dirac cone picture. This conclusion is in line with ARPES results [9], as depicted by the two-cone picture in Fig. 2(a). In turn, this gives rise to the two-step absorption feature of the optical conductivity. We also like to point out that even the high-temperature spectra reveal signatures of these two step absorption feature. In Fig. 2(b), the $T = 300$ and 150 K spectra are given for comparison; the steps due to the Dirac bands are marked by colored dots.

From our spectrum at $T = 7$ K we estimate the positions of the Dirac points at $E_{D1} = 346$ cm^{-1} (42 meV) and $E_{D2} = 983$ cm^{-1} (122 meV); they do not change significantly with temperature. These values are well in line with ARPES measurements [9], while they do not consider the correlation gap observed in ARPES. Such an energy gap due to correlated Dirac fermions resembles the optical response known from density-wave systems [25]. However, in the present case we should not see such an effect, as the gap is buried well below E_F.

Let us turn to the low-lying absorption band of the spectra. We associate these features with the response of the flat bands, since they are located in the vicinity of the Fermi energy. We can identify several absorption features in the spectra at 72, 141, 172, 223, 311, 542 cm^{-1}; however, a close look reveals that most of them do not shift with decreasing temperature, but they simply get sharper [marked by the arrows in Fig. 1(b)]. We attribute these peaks to van Hove singularities of the flat bands. As shown by STM measurements [6], flat bands do not extend over the entire Brillouin zone. They possess a small dispersion giving rise to several peaks in the density of states around the Fermi energy. Due to the band dispersion, the transitions across the Fermi energy between these flat bands occur at slightly different energies, as observed.

The absorption feature around 100 cm^{-1} is by far the most prominent one with a distinct dynamics: it changes its shape and strongly shifts in energy upon cooling. Our detailed analysis reveals that this feature is strongly linked to the underlying magnetic structure. Fe_3Sn_2 possesses flatband ferromagnetism related to the underlying kagome lattice with a ferromagnetic phase transition at $T_C = 640$ K. Previous magnetization, neutron diffraction, and Mössbauer spectroscopy studies all conclude that the spins are canted towards out of plane at high temperatures up to T_C. With decreasing temperature they tend to reorient towards the kagome plane [26–29]. However, no agreement has been reached on the temperature range, where this reorientation occurs, and whether the phase transition is of a first or a second order. A recent magnetotransport study showed that the spin reorientation takes place in a temperature range between 70–150 K with a transition peak at $T = 120$ K [16]. The nature of this spin reorientation and its implications on the electronic structure remain to be clarified. Characterizing our sample in this regard, in Fig. 3(a) we plot the magnetic susceptibility as a function of temperature. Our findings are consistent with the literature and yield a crossover temperature slightly below 150 K [17].

Let us turn back to the strong optical absorption around 100 cm^{-1}. To better analyze the evolution of the peak, we plotted the relative optical conductivity $[\sigma_1(T)/\sigma_1(300K)]$ in Fig. 3(b), where one can trace the energy position of the peak as well as the transfer of spectral weight to the low-lying absorption features. Although we cannot rule out completely that appear accidentally, at elevated temperatures a clear isosbestic point (indicated by the red symbols, crossing of the spectra at 300 K spectrum, see the Supplemental Material [17] for the details) of the spectra can be defined along with the SW transfer that is lead by the temperature change [32]. Below the spin reorientation temperature the isosbestic behavior does not hold anymore and the spectra crossing point rapidly shifts to the smaller energies, as the SW accumulates to a very sharp peak structure. From Fig. 3(c) we can see that its maximum (green circles) gradually moves to lower energies: while for $T > 150$ K it decreases linearly in T, the shift tends to saturate at lower temperatures. The drastic change of the isosbestic signature suggests the influence of another mechanism other than the temperature on the SW redistribution.

Since the flat bands possess strongly correlated, localized charge carriers, the so-called localization peak is a plausible assumption for the observed peak. The generalization of the Drude response is commonly discussed in the framework of the strongly correlated electron systems [30,31,33]. The partial localization of the charge carriers leads to a displaced Drude peak, where the low-energy part of the optical conductivity is strongly suppressed and the peaklike structure appears at finite energies. Literature is rich in this regard,

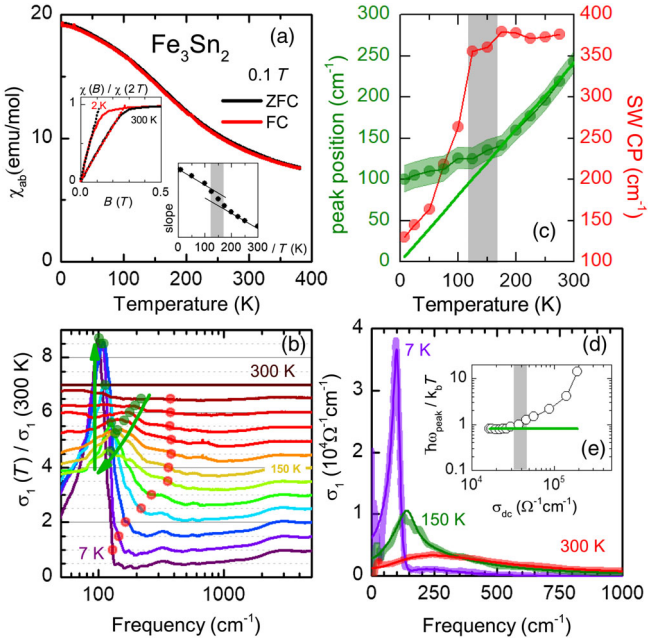

FIG. 3. (a) Magnetic susceptibility of Fe_3Sn_2 measured for $H||ab$ plane in field-cooled and zero-field-cooled configuration. The inset shows the field dependence $\chi(B)$ normalized to 2 T value (above the saturation field) for $T = 300$ and 2 K. Also shown is the slope of the low-field magnetization as a function of T indicating the spin-reorientation transition. (b) Relative optical conductivity normalized to the room temperature spectrum. The spectra for $T > 7$ K are shifted by 0.5 each with respect to each other. The red circles mark the point where the spectra cross each other, indicating the spectral weight transfer energy. The green circles are the maximum of the low-lying absorption feature shifting in energy. Green arrows are guide to the eye following the decreasing temperature. Panel (c) shows the T dependence of the red and green circles in panel (b). The solid green line represent the position of the expected localization peak extended to the lower temperatures, highlighting the clear deviation. The same scaling also given in panel (e). (d) Energy-dependent absorption feature at $T = 300$, 150, and 7 K with the localization peak fit from reference [30]. (e) Scaling of the peak position with the dc conductivity suggested by [31]. Grey shaded areas in figures represent the crossover temperature, where the spin reorientation takes place.

with examples from numerous transition metal oxides [34–44] and organic conductors [45,46]. Please note that the phenomenological descriptions of the optical conductivity does not rely on any specific nature of the localization, but generally discussed in terms of disorder effects. Here, we employed the model proposed by Fratini *et al.*, where the low-energy Drude response is modified with the electron backscattering [30,46], while the high-energy tail of the modified Drude response is still defined with the elastic scattering rate of the free carriers [17]. These optical fingerprints commonly go hand in hand with a linear-in-T resistivity (so-called bad metallic behavior), where the shift of the peak scales with the dc conductivity [31].

To better demonstrate the phenomenological description of the peak in Fig. 3(d), we subtract the response of the Dirac bands, as well as the van-Hove singularities from the measured optical conductivity. The solid lines are the best fits to the model suggested by Fratini *et al.* [30]. The high-temperature data are well reproduced by taking into account the backscattering correction, where we restrict ourselves with the static limit. We estimate the backscattering time of the electrons, τ_b, to be around 13 fs at room temperature and increases to 76 fs at $T = 150$ K. Below the transition at 150 K, the description breaks down: the observed feature corresponds to a very sharp Fano-like peak rather than a modified Drude peak. This is in accord with the breakdown of the scaling relation between the dc conductivity and the linear shift of the peak energy below 150 K, displayed in Fig. 3(e). Indeed, the presence of spin reorientation calls for a different approach at low temperatures. A better accuracy can be satisfied by taking into account a coupling of a Fano resonance to the electronic background. The Fano resonance starts to appear below ~150 K and gets more pronounced with decreasing temperature. Along with a stronger coupling to the electronic background, the behavior of the Fano resonance follows the magnetization of the sample and the spin reorientation [17].

The appearance of such a sharp peak resembles excitations between electronic bands at E_F; i.e., it suggests the development of a partial gap in the density of states. This can be explained by additional Weyl nodes recently predicted for Fe_3Sn_2 [12]. Their existence is linked to the spin directions of the iron atoms within the kagome plane. When the spins reorient within the plane, the Weyl nodes become gapped for a certain direction of magnetization, while, for the other in-plane direction, there should be no gap. Hence, we conclude that the spin reorientation to the in-plane direction opens up the gap at the Weyl points, which we detect by optical means. The gap energy estimated from our measurements is 98 cm^{-1} (12 meV), which is in accord with the gap energy expected from calculations [12].

It is not surprising that these Weyl nodes are not identified by ARPES, because the current optical measurements possess a much higher energy resolution. Moreover, since the magnetic properties and the electronic structure are very sensitive to small fields, signatures of the gap might be missed in the magnetotransport measurements. The current optical study was conducted in a zero field, taking into account only the inherent magnetization of the compound. This allows us to discover experimentally the proposed gap opening.

In summary, temperature and frequency-dependent infrared studies on the magnetic kagome metal Fe_3Sn_2 reveal optical fingerprints of strongly correlated flat bands and topologically nontrivial Dirac fermions. The two-step absorption feature that evolves in the frequency-independent optical conductivity indicates the existence of

two-dimensional Dirac cones shifted in energy with respect to each other. The flat bands are seen as multiple absorption peaks in the low-energy optical conductivity. One of the peaks exhibits a strong shift in energy. At high temperatures, this peak reveals striking similarities with the displaced Drude peak as an indication of localization effects. Below the spin reorientation temperature around 120 K, a gap opens around the Fermi energy as a signature for theoretically proposed gapped Weyl nodes. On the other hand, spin reorientation seems not to effect the Dirac nodes buried well into the Fermi energy.

The authors acknowledge fruitful discussions with L. Z. Maulana and A. V. Pronin and the technical support by G. Untereiner. H. C. L. acknowledges support from the National Key R&D Program of China (Grants No. 2016YFA0300504 and No. 2018YFE0202600), and the National Natural Science Foundation of China (Grants No. 11574394, No. 11774423, and No. 11822412). The work has been supported by the Deutsche Forschungsgemeinschaft (DFG) via Grants No. DR228/48-1 and No. DR228/51-1. E. U. acknowledges the European Social Fund and the Baden-Württemberg Stiftung for the financial support of this research project by the Eliteprogramme.

*hlei@ruc.edu.cn
†ece.uykur@pi1.physik.uni-stuttgart.de

[1] D. F. Liu, A. J. Liang, E. K. Liu, Q. N. Xu, Y. W. Li, C. Chen, D. Pei, W. J. Shi, S. K. Mo, P. Dudin, T. Kim, C. Cacho, G. Li, Y. Sun, L. X. Yang, Z. K. Liu, S. S. P. Parkin, C. Felser, and Y. L. Chen, Magnetic Weyl semimetal phase in a Kagomé crystal, Science **365**, 1282 (2019).

[2] S. Nakatsuji, N. Kiyohara, and T. Higo, Large anomalous Hall effect in a non-collinear antiferromagnet at room temperature, Nature (London) **527**, 212 (2015).

[3] A. K. Nayak, J. E. Fischer, Y. Sun, B. Yan, J. Karel, A. C. Komarek, C. Shekhar, N. Kumar, W. Schnelle, J. Kübler, C. Felser, and S. S. P. Parkin, Large anomalous Hall effect driven by a nonvanishing Berry curvature in the noncolinear antiferromagnet Mn_3Ge, Sci. Adv. **2**, e1501870 (2016).

[4] E. Liu, Y. Sun, N. Kumar, L. Muechler, A. Sun, L. Jiao, S.-Y. Yang, D. Liu, A. Liang, Q. Xu, J. Kroder, V. S, H. Borrmann, C. Shekhar, Z. Wang, C. Xi, W. Wang, W. Schnelle, S. Wirth, Y. Chen, S. T. B. Goennenwein, and C. Felser, Giant anomalous Hall effect in a ferromagnetic kagome-lattice semimetal, Nat. Phys. **14**, 1125 (2018).

[5] Q. Xu, E. Liu, W. Shi, L. Muechler, J. Gayles, C. Felser, and Y. Sun, Topological surface Fermi arcs in the magnetic Weyl semimetal $Co_3Sn_2S_2$, Phys. Rev. B **97**, 235416 (2018).

[6] Z. Lin, J.-H. Choi, Q. Zhang, W. Qin, S. Yi, P. Wang, L. Li, Y. Wang, H. Zhang, Z. Sun, L. Wei, S. Zhang, T. Guo, Q. Lu, J.-H. Cho, C. Zeng, and Z. Zhang, Flatbands and Emergent Ferromagnetic Ordering in Fe_3Sn_2 Kagome Lattices, Phys. Rev. Lett. **121**, 096401 (2018).

[7] Q. Wang, S. Sun, X. Zhang, F. Pang, and H. Lei, Anomalous Hall effect in a ferromagnetic Fe_3Sn_2 single crystal with a geometrically frustrated Fe bilayer kagome lattice, Phys. Rev. B **94**, 075135 (2016).

[8] H. Li, B. Ding, J. Chen, Z. Li, Z. Hou, E. Liu, H. Zhang, X. Xi, G. Wu, and W. Wang, Large topological Hall effect in a geometrically frustrated kagome magnet Fe_3Sn_2, Appl. Phys. Lett. **114**, 192408 (2019).

[9] L. Ye, M. Kang, J. Liu, F. von Cube, C. R. Wicker, T. Suzuki, C. Jozwiak, A. Bostwick, E. Rotenberg, D. C. Bell, L. Fu, R. Comin, and J. G. Checkelsky, Massive Dirac fermions in a ferromagnetic kagome metal, Nature (London) **555**, 638 (2018).

[10] J.-X. Yin, S. S. Zhang, H. Li, K. Jiang, G. Chang, B. Zhang, B. Lian, C. Xiang, I. Belopolski, H. Zheng, T. A. Cochran, S.-Y. Xu, G. Bian, K. Liu, T.-R. Chang, H. Lin, Z.-Y. Lu, Z. Wang, S. Jia, W. Wang, and M. Z. Hasan, Giant and anisotropic many-body spin-orbit tunability in a strongly correlated kagome magnet, Nature (London) **562**, 91 (2018).

[11] Z.-Z. Lin and X. Chen, Tunable massive dirac fermions in ferromagnetic Fe_3Sn_2 kagome lattice, Phys. Status Solidi (RRL) **14**, 1900705 (2020).

[12] M. Yao, H. Lee, N. Xu, Y. Wang, J. Ma, O. V. Yazyev, Y. Xiong, M. Shi, G. Aeppli, and Y. Soh, Switchable Weyl nodes in topological kagome ferromagnet Fe_3Sn_2, arXiv:1810.01514.

[13] A. Mielke, Ferromagnetic ground states for the Hubbard model on line graphs, J. Phys. A **24**, L73 (1991).

[14] A. Mielke, Ferromagnetism in the Hubbard model on line graphs and further considerations, J. Phys. A **24**, 3311 (1991).

[15] A. Mielke, Exact ground states for the Hubbard model on the kagome lattice, J. Phys. A **25**, 4335 (1992).

[16] N. Kumar, Y. Soh, Y. Wang, and Y. Xiong, Magnetotransport as a diagnostic of spin reorientation: Kagome ferromagnet as a case study, Phys. Rev. B **100**, 214420 (2019).

[17] See the Supplemental Material at http://link.aps.org/supplemental/10.1103/PhysRevLett.125.076403 for more details on the crystals, experiments and analysis, magnetic characterization, spectral weight analysis, and decomposition, including Refs. [18–20].

[18] M. Dressel and G. Grüner, *Electrodynamics of Solids: Optical Properties of Electrons in Matter* (Cambridge University Press, New York, 2002).

[19] D. B. Tanner, Use of x-ray scattering functions in Kramers-Kronig analysis of reflectance, Phys. Rev. B **91**, 035123 (2015).

[20] U. Fano, Effects of configuration interaction on intensities and phase shifts, Phys. Rev. **124**, 1866 (1961).

[21] It is interesting to examine the scattering rate of this sharp Drude component. The momentum-relaxing scattering of the free carriers (in the current case is the Dirac fermions as explained in the text) can be observed in the optical conductivity. Hence, one can directly obtain the corresponding scattering time, τ, from the real part of the optical conductivity, $\sigma_1(\omega)$. The simultaneous fits of the reflectivity and the optical conductivity of our low energy Drude component reveals a scattering rate $[\gamma = 1/(2\pi c\tau)]$ of 2 cm^{-1} at 7 K, while it increases to $\sim$17 cm^{-1} at room temperature. These corresponds to the scattering times

$\tau_{7K} = 2.5$ ps and $\tau_{300K} = 0.3$ ps. Considering the reported average Fermi velocity for Fe_3Sn_2, $v_F = 2.2 \times 10^5$ m/s, the momentum relaxation lengths [$\ell = v_F\tau$] are calculated as $\ell_{7K} = 0.55$ μm and $\ell_{300K} = 66$ nm. Considering that the localized carrier response of the flat bands are separated in energy and does not contribute to the low energy dynamics (within the obtained scattering scales), these length scales suggest that Fe_3Sn_2 readily might be a suitable platform to realize a ballistic transport.

[22] Z. Q. Li, E. A. Henriksen, Z. Jiang, Z. Hao, M. C. Martin, P. Kim, H. L. Störmer, and D. N. Basov, Dirac charge dynamics in graphene by infrared spectroscopy, Nat. Phys. **4**, 532 (2008).

[23] B. Scharf, V. Perebeinos, J. Fabian, and P. Avouris, Effects of optical and surface polar phonons on the optical conductivity of doped graphene, Phys. Rev. B **87**, 035414 (2013).

[24] V. P. Gusynin, S. G. Sharapov, and J. P. Carbotte, Unusual Microwave Response of Dirac Quasiparticles in Graphene, Phys. Rev. Lett. **96**, 256802 (2006).

[25] E. Uykur, W. Li, C. A. Kuntscher, and M. Dressel, Optical signatures of energy gap in correlated Dirac fermions, npj Quantum Mater. **4**, 19 (2019).

[26] G. Trumpy, E. Both, C. Djéga-Mariadassou, and P. Lecocq, Mössbauer-effect studies of iron-tin alloys, Phys. Rev. B **2**, 3477 (1970).

[27] G. L. Caer, B. Malaman, and B. Roques, Mossbauer effect study of Fe_3Sn_2, J. Phys. F **8**, 323 (1978).

[28] B. Malaman, D. Fruchart, and G. L. Caer, Magnetic properties of Fe_3Sn_2. II. Neutron diffraction study (and Mossbauer effect), J. Phys. F **8**, 2389 (1978).

[29] G. L. Caer, B. Malaman, L. Haggstrom, and T. Ericsson, Magnetic properties of Fe_3Sn_2. III. A ^{119}Sn Mossbauer study, J. Phys. F **9**, 1905 (1979).

[30] S. Fratini, S. Ciuchi, and D. Mayou, Phenomenological model for charge dynamics and optical response of disordered systems: Application to organic semiconductors, Phys. Rev. B **89**, 235201 (2014).

[31] L. V. Delacrtaz, B. Goutraux, S. A. Hartnoll, and A. Karlsson, Bad metals from fluctuating density waves, SciPost Phys. **3**, 025 (2017).

[32] M. Greger, M. Kollar, and D. Vollhardt, Isosbestic points: How a narrow crossing region of curves determines their leading parameter dependence, Phys. Rev. B **87**, 195140 (2013).

[33] N. V. Smith, Classical generalization of the Drude formula for the optical conductivity, Phys. Rev. B **64**, 155106 (2001).

[34] P. Kostic, Y. Okada, N. C. Collins, Z. Schlesinger, J. W. Reiner, L. Klein, A. Kapitulnik, T. H. Geballe, and M. R. Beasley, Non-Fermi-Liquid Behavior of $SrRuO_3$: Evidence from Infrared Conductivity, Phys. Rev. Lett. **81**, 2498 (1998).

[35] Y. S. Lee, J. Yu, J. S. Lee, T. W. Noh, T.-H. Gimm, H.-Y. Choi, and C. B. Eom, Non-Fermi liquid behavior and scaling of the low-frequency suppression in the optical conductivity spectra of $CaRuO_3$, Phys. Rev. B **66**, 041104(R) (2002).

[36] C. Bernhard, A. V. Boris, N. N. Kovaleva, G. Khaliullin, A. V. Pimenov, L. Yu, D. P. Chen, C. T. Lin, and B. Keimer, Charge Ordering and Magnetopolarons in $Na_{0.82}CoO_2$, Phys. Rev. Lett. **93**, 167003 (2004).

[37] N. L. Wang, P. Zheng, D. Wu, Y. C. Ma, T. Xiang, R. Y. Jin, and D. Mandrus, Infrared Probe of the Electronic Structure and Charge Dynamics of $Na_{0.7}CoO_2$, Phys. Rev. Lett. **93**, 237007 (2004).

[38] A. V. Puchkov, T. Timusk, S. Doyle, and A. M. Hermann, ab-plane optical properties of $Tl_2Ba_2CuO_{6+\delta}$, Phys. Rev. B **51**, 3312 (1995); J. Hwang, T. Timusk, and G. D. Gu, Doping dependent optical properties of $Bi_2Sr_2CaCu_2O_8$, J. Phys. Condens. Matter **19**, 125208 (2007).

[39] A. A. Tsvetkov, J. Schützmann, J. I. Gorina, G. A. Kaljushnaia, and D. van der Marel, In-plane optical response of $Bi_2Sr_2CuO_6$, Phys. Rev. B **55**, 14152 (1997).

[40] T. Osafune, N. Motoyama, H. Eisaki, S. Uchida, and S. Tajima, Pseudogap and Collective Mode in the Optical Conductivity Spectra of Hole-Doped Ladders in $Sr_{14-x}Ca_xCu_{24}O_{41}$, Phys. Rev. Lett. **82**, 1313 (1999); E. Uykur, K. Tanaka, T. Masui, S. Miyasaka, and S. Tajima, In-plane optical spectra of $Y_{1-x}Ca_xBa_2Cu_3O_{7-\delta}$: Overdoping and disorder effects on residual conductivity, Phys. Rev. B **84**, 184527 (2011).

[41] M. J. Rozenberg, G. Kotliar, H. Kajueter, G. A. Thomas, D. H. Rapkine, J. M. Honig, and P. Metcalf, Optical Conductivity in Mott-Hubbard Systems, Phys. Rev. Lett. **75**, 105 (1995).

[42] P. E. Jönsson, K. Takenaka, S. Niitaka, T. Sasagawa, S. Sugai, and H. Takagi, Correlation-Driven Heavy-Fermion Formation in LiV_2O_4, Phys. Rev. Lett. **99**, 167402 (2007).

[43] K. Takenaka, Y. Sawaki, and S. Sugai, Incoherent-to-coherent crossover of optical spectra in $La_{0.825}Sr_{0.175}MnO_3$: Temperature-dependent reflectivity spectra measured on cleaved surfaces, Phys. Rev. B **60**, 13011 (1999); K. Takenaka, R. Shiozaki, and S. Sugai, Charge dynamics of a double-exchange ferromagnet $La_{1-x}Sr_xMnO_3$, Phys. Rev. B **65**, 184436 (2002).

[44] R. Jaramillo, S. D. Ha, D. M. Silevitch, and S. Ramanathan, Origins of bad-metal conductivity and the insulator-metal transition in the rare-earth nickelates, Nat. Phys. **10**, 304 (2014).

[45] J. Dong, J. L. Musfeldt, J. A. Schlueter, J. M. Williams, P. G. Nixon, R. W. Winter, and G. L. Gard, Optical properties of β''-$(ET)_2SF_5CH_2CF_2SO_3$: A layered molecular superconductor with large discrete counterions, Phys. Rev. B **60**, 4342 (1999).

[46] K. Takenaka, M. Tamura, N. Tajima, H. Takagi, J. Nohara, and S. Sugai, Collapse of Coherent Quasiparticle States in θ-$(BEDT\text{-}TTF)_2I_3$ Observed by Optical Spectroscopy, Phys. Rev. Lett. **95**, 227801 (2005); S. Fratini, D. Mayou, and S. Ciuchi, The transient localization scenario for charge transport in crystalline organic materials, Adv. Funct. Mater. **26**, 2292 (2016); S. Fratini and S. Ciuchi, Dynamical localization corrections to band transport, Phys. Rev. Research **2**, 013001 (2020).